

IAC-15.C1.2.6**SOLAR SAILING WITH INVARIANT MANIFOLDS IN THE EARTH-SUN SYSTEM**

Ariadna Farrés

Universitat de Barcelona, Spain, ariadna.farres@maia.ub.es

Àngel Jorba

Universitat de Barcelona, Spain, angel@maia.ub.es

Abstract

Solar sails are extremely interesting for long interplanetary transfers, but also offer many advantages in Libration Point Orbits (LPO) missions. The extra effect of the SRP allows us, by changing the sail orientation, to artificially displace the classical Lagrangian equilibrium points, L_1, \dots, L_5 , as well as the Lyapunov, Halo and Lissajous orbits that appear around them. Most of these points are linearly unstable and have stable and unstable invariant manifolds associated to them. In this paper we want to explore the possibilities that these invariant manifolds offer for navigating in a natural way around the system. We will use the Earth-Sun Restricted Three Body Problem (RTBP) as a model and, for different fixed sail orientations, we will compute the stable and unstable manifolds associated to the equilibrium points of the system. We want to find natural trajectories that allow us to move around the family of equilibria in a controlled way, going from a region close to L_1 to a region close to L_2 or even L_4 and L_5 .

I. INTRODUCTION

Solar sailing is a spacecraft propulsion system, that uses large reflecting surfaces to take advantage of the solar radiation pressure (SRP) enabling a constant acceleration, and therefore a potentially unlimited thrust. This offers the opportunity to combine low-cost operations with long-term missions.

The successful deployment of a solar sail by IKAROS (December 2010) by JAXA^a NanoSail-D2 (January 2011) by NASA^b and recently Light Sail (June 2015) by the Planetary Society^c have finally validated the concept of solar sailing. Unfortunately there has not been yet any operational mission using solar sails.

Nevertheless many studies on this new propulsion system are being conducted by the scientific community. From the point of view of astrodynamics and mission applications, solar sails are being considered for:

- the Sunjammer mission, an enhanced warning missions to detect the solar magnetic storms, the solar sail allows to displaced the Lagrangian equilibrium points.⁸
- as drag-sails to accelerate the de-orbiting rate of LEO satellites¹⁵ and as an end-of-life strategy in LPOs.¹³
- a low-cost multi NEO rendezvous mission, the mission

could visit many asteroids and be flexible in the selected destinations.²

In this paper we want to explore the structure of invariant manifolds that exist in the Restricted Three Body Problem (RTBP) and use it to derive transfer orbits between different regions in the phase space. The stable and unstable invariant manifolds in the RTBP have already been used to provide cheap transfer orbit between the Earth and a Halo orbits, and their potential for chemical propulsion systems has been widely studied.⁹

To model the dynamics of a solar sail in the Earth-Sun system we will consider the RTBP adding the effect of the solar radiation pressure due to the solar sail. The acceleration given by the solar sail depends on three parameters: β , known as the sail lightness number, that measures the sail efficiency, and α, δ two angles measuring the orientation of the sail. It is well known that the extra effect of the solar sail in the RTBPS allows us to “artificially” displace the Lagrangian equilibrium points ($L_{1,\dots,5}$) having for a given β a 2D family of equilibrium points.

We have computed these families of equilibrium points for different sail configurations ($\beta = 0.01, 0.02, 0.03, 0.04$ and 0.05). In section V. we will describe these families of equilibrium points and classify them regarding their stability. These equilibrium points offer privileged positions in the phase space for observational missions and have been proposed missions such as Sunjammer⁸ or the Polar Observer.¹ We will see that many of them are unstable and have stable and unstable manifolds associated to them. This invariant manifolds can be used to find natural

^a<http://www.isas.jaxa.jp/e/enterp/missions/ikaros/index.shtml>

^bhttp://www.nasa.gov/mission_pages/smallsats/nanosaild.html

^c<http://sail.planetary.org>

transfer trajectories from one point to another in the phase space.

In section VI. we will describe the invariant manifolds that appear around some of the artificial equilibrium points. We will focus on three different mission applications. The first application (section VI.I) will be to use the linear approximation of these manifolds to find a strategy to drift along the family of equilibria in a controlled way. The second application (section VI.II) will be to study the feasibility of transferring a solar sail from the L_1 region to the L_2 region. Finally, the third application (section VI.III) will be to use the solar sail to gain enough energy to transfer from L_1 or L_2 to a neighbourhood of L_4 .

II. EQUATIONS OF MOTION

To describe the motion of a solar sail in the Earth - Sun system we consider as a model the Circular Restricted Three Body Problem (RTBP) adding the Solar Radiation Pressure (SRP) due to the solar sail (RTBPS). We assume that the Earth and Sun are point masses moving around their common centre of mass in a circular way due to their mutual gravitational attraction. The solar sail on the other hand is a mass-less particle that does not affect the motion of the two primaries but is affected by their gravitational attraction as well as the SRP.

We normalise the units of mass, distance and time, so that the total mass of the system is 1, the Earth - Sun distance is 1 and the period of its orbit is 2π . In this units the universal gravitational constant $G = 1$, the mass of the Earth is $\mu = 3.0034806 \times 10^{-6}$, and $1 - \mu$ corresponds to the mass of the Sun. We use a synodic reference system with the origin at the centre of mass of the Earth - Sun system and such that the Earth and Sun are fixed on the x -axis (with its positive side pointing towards the Sun), the z -axis is perpendicular to the ecliptic plane and the y -axis completes an orthogonal positive oriented reference system.¹⁴

Within these assumptions, the equations of motion in the synodic reference system are:

$$\begin{aligned}\ddot{x} - 2\dot{y} &= x + (1 - \mu) \frac{x - \mu}{r_{ps}^3} + \mu \frac{x - \mu + 1}{r_{pe}^3} + a_x, \\ \ddot{y} + 2\dot{x} &= y + \left(\frac{1 - \mu}{r_{ps}^3} + \frac{\mu}{r_{pe}^3} \right) y + a_y, \\ \ddot{z} &= \left(\frac{1 - \mu}{r_{ps}^3} + \frac{\mu}{r_{pe}^3} \right) z + a_z,\end{aligned}\quad (1)$$

where $\mathbf{a} = (a_x, a_y, a_z)$ is the acceleration given by the solar sail, and $r_{ps} = \sqrt{(x - \mu)^2 + y^2 + z^2}$, $r_{pe} = \sqrt{(x - \mu + 1)^2 + y^2 + z^2}$ are the Sun-sail and Earth-sail distances respectively.

III. THE SOLAR SAIL ACCELERATION

The acceleration given by the solar sail depends on its efficiency defined by the **sail lightness number** β , and its **orientation** parametrised by two angles α, δ . In this paper we will consider the simplest model for a solar sail, we assume it to be flat and perfectly reflecting. Hence, the acceleration due to the SRP is in the normal direction to the surface of the solar sail. For a more

realistic model one should also take into account the absorption of the photons by the surface of the sail. In this case, an extra component in the transverse direction to the sail must be added which will slightly changing the efficiency of the sail and the direction of the acceleration vector.³

The force produced by the reflected photons is given by $\mathbf{F}_r = 2PA\langle \mathbf{n}, \mathbf{r}_s \rangle^2 \mathbf{n}$, where $P = P_0(R_0/R)^2$ is the SRP magnitude at a distance R from the Sun (being $P_0 = 4.563\text{N/m}^2$ is the SRP magnitude at $R_0 = 1\text{AU}$), A is the area of the solar sail, \mathbf{r}_s is the Sun-sail direction and \mathbf{n} is the normal direction to the surface of the sail (both unit vector). As the SRP is proportional to the inverse square of the distance to the Sun it is common to write its effect as a correction of the Sun's gravitational attraction:

$$\mathbf{a} = \beta \frac{(1 - \mu)}{r_{ps}^2} \langle \mathbf{r}_s, \mathbf{n} \rangle^2 \mathbf{n}, \quad (2)$$

where β corresponds to the sail lightness number, which accounts for the sail's effectiveness. One can also interpret β as the ratio between the gravitational attraction and the solar sail acceleration.

It can be seen that,

$$\beta = \sigma^*/\sigma, \quad \sigma^* = \frac{2P_0R_0^2}{Gm_s} = 1.53\text{g/m}^2,$$

where $\sigma = m/A$ is the area-to-mass ratio of the solar sail.¹¹ This means that, for instance, a sail lightness number $\beta = 0.03$ corresponds to a characteristic acceleration of $a_0 = 0.179804\text{mm/s}^2$. Moreover, if we have a payload mass of 10kg we need a solar sail area of almost $14 \times 14\text{m}^2$ to have a sail lightness number $\beta = 0.03$. In Table 1 we can see for different sail lightness numbers β , the corresponding area-to-mass ration (σ), the characteristic acceleration and the size of the solar sail if we have a 10kg payload.

β	$\sigma (\text{g/m}^2)$	$a_0(\text{mm/s}^2)$	Area (m^2)
0.01	153.0	0.059935	$\approx 8 \times 8$
0.02	76.5	0.119869	$\approx 12 \times 12$
0.03	51.0	0.179804	$\approx 14 \times 14$
0.04	38.25	0.239739	$\approx 16 \times 16$
0.05	30.6	0.359608	$\approx 20 \times 20$

Table 1: Relation between the sail lightness number β and: the area-to-mass ration of the satellite (σ), the characteristic acceleration (a_0), and the area requirements for the solar sail if the have a 10kg payload satellite.

The **sail orientation** is given by the normal direction to the surface of the sail, $\mathbf{n} = (n_x, n_y, n_z)$, and is parametrised by two angles α and δ that measure the displacement of \mathbf{n} with respect to the Sun-sail direction $\mathbf{r}_s = (x - \mu, y, z)/r_{ps}$. Following¹⁰ we can define the normal direction to the surface of the sail as:

$$\begin{aligned}n_x &= \frac{x - \mu}{r_{ps}} \cos \alpha - \frac{(x - \mu)z}{r_2 r_{ps}} \sin \alpha \cos \delta + \frac{y}{r_2} \sin \alpha \sin \delta, \\ n_y &= \frac{y}{r_{ps}} \cos \alpha - \frac{yz}{r_2 r_{ps}} \sin \alpha \cos \delta - \frac{x - \mu}{r_2} \sin \alpha \sin \delta, \\ n_z &= \frac{z}{r_{ps}} \cos \alpha + \frac{r_2}{r_{ps}} \sin \alpha \cos \delta,\end{aligned}\quad (3)$$

where $r_2 = \sqrt{(x - \mu)^2 + z^2}$, α corresponds to the pitch angle (angle between \mathbf{n} and \mathbf{r}_s) and δ the clock angle (angle given by the projection of \mathbf{n} in an orthogonal plane to \mathbf{r}_s).

Notice that the the normal vector to the surface of the sail, \mathbf{n} , cannot point towards the Sun, hence $\langle \mathbf{n}, \mathbf{r}_s \rangle > 0$ implying that $\alpha, \delta \in [-\pi/2 : \pi/2]$.

IV. THE JACOBI CONSTANT

From a mathematical point of view the Earth-Sun-Sail RTBPS can be seen as a perturbation of the Earth-Sun RTBP, where the perturbation destroys the Hamiltonian structure of the system. From previous works^{4,6} we know that for $\alpha = \delta = 0$ (i.e. the solar sail perpendicular to the Sun-sail line) the system is Hamiltonian and for $\alpha \neq 0, \delta = 0$ (i.e. the orientation of the solar sail varies vertically w.r.t. the Sun-sail line) the system is Time-Reversible. In this two particular cases we can ensure that around an equilibrium point (for a fixed sail orientation) we have periodic and quasi-periodic motion.

One of the interesting properties of Hamiltonian systems is that they have at least one first integral, i.e. a function which is conserved through time. In the case of the RTBP we have the well known Jacobi constant, that can also be seen as the energy level of the system. This function is usually used to classify possible regions of motion.

In the case of the RTBPS, for a fixed sail orientation, we do not have the concept a Jacobi constant or energy level. But we would like to define a function that allowed us to classify the type of motions. Notice that taking Eq. 1 and Eq. 3 we can write the equations of motion for the solar sail as:

$$\begin{aligned} \ddot{x} - 2\dot{y} &= \frac{\partial \tilde{\Omega}}{\partial x} + \beta \frac{1-\mu}{r_{ps}^2} \cos^2 \alpha \left(\frac{-(x-\mu)z}{r_2 r_{ps}} \sin \alpha \cos \delta \right. \\ &\quad \left. + \frac{y}{r_2} \sin \alpha \sin \delta \right), \\ \ddot{y} + 2\dot{x} &= \frac{\partial \tilde{\Omega}}{\partial y} + \beta \frac{1-\mu}{r_{ps}^2} \cos^2 \alpha \left(\frac{-yz}{r_2 r_{ps}} \sin \alpha \cos \delta \right. \\ &\quad \left. - \frac{x-\mu}{r_2} \sin \alpha \sin \delta \right), \\ \ddot{z} &= \frac{\partial \tilde{\Omega}}{\partial z} + \beta \frac{1-\mu}{r_{ps}^2} \cos^2 \alpha \left(\frac{r_2}{r_{ps}} \sin \alpha \cos \delta \right), \end{aligned} \quad (4)$$

where $\tilde{\Omega}(x, y, z) = \frac{1}{2}(x^2 + y^2) + (1 - \beta \cos^3 \alpha) \frac{1-\mu}{r_{ps}} + \frac{\mu}{r_{pe}}$, and we can define and approximate energy level,

$$\tilde{J}_c = \dot{x}^2 + \dot{y}^2 + \dot{z}^2 - 2\tilde{\Omega}(x, y, z). \quad (5)$$

Notice that for $\beta = 0$ (i.e. no sail) or if $\alpha = 0, \delta = 0$ (a sail perpendicular to the Sun-sail line), this function corresponds to the Jacobi constant of the RTBP or RTBPS (Hamiltonian case).

If we look at the variation of this function over time, we have:

$$\begin{aligned} \frac{d\tilde{J}_c}{dt} &= \beta \frac{(1-\mu)}{r_{ps}^2} \cos^2 \alpha \sin \alpha \left(\frac{\dot{xy} - \dot{y}(x-\mu)}{r_2} \sin \delta \right. \\ &\quad \left. + \frac{r_2^2 \dot{z} - ((x-\mu)\dot{x} + y\dot{y})z}{r_{ps} r_2} \cos \delta \right). \end{aligned}$$

This expression can give us an idea on how the energy of the system varies. Notice that, as expected, \tilde{J}_c is constant for $\alpha = 0$ or $\beta = 0$, and for $\alpha \approx 0$ this variation will be small. We will also use this “constant” to decide if a transfer trajectory between two equilibrium points is feasible or not.

In the Hamiltonian case, $\alpha = 0$, the constant \tilde{J}_c helps us find the region of possible motion. Notice that $\tilde{J}_c = \|\mathbf{v}\|^2 - 2\tilde{\Omega}(x, y, z)$, hence the region of possible motion is defined by $(x, y, z) \in \mathbb{R}^3$ such that $\tilde{J}_c + 2\tilde{\Omega}(x, y, z) \geq 0$. The zero velocity curves $\mathcal{ZV}(J_c) = \{(x, y, z) \in \mathbb{R}^3 \mid J_c + 2\tilde{\Omega}(x, y, z) = 0\}$ define the frontier between allowed and not allowed motion.

In Fig. 1 we plot the zero velocity curves for $\beta = 0$ (top) and $\beta = 0.01$ (bottom) in the region close to L_1, L_2 points. We can see how the structure varies drastically as we increase the value of β . For $\beta = 0$ the required energy level to have motion around L_1 and L_2 is almost the same, while for $\beta = 0.01$ we have motion around L_2 for a lower energy level than for L_1 .

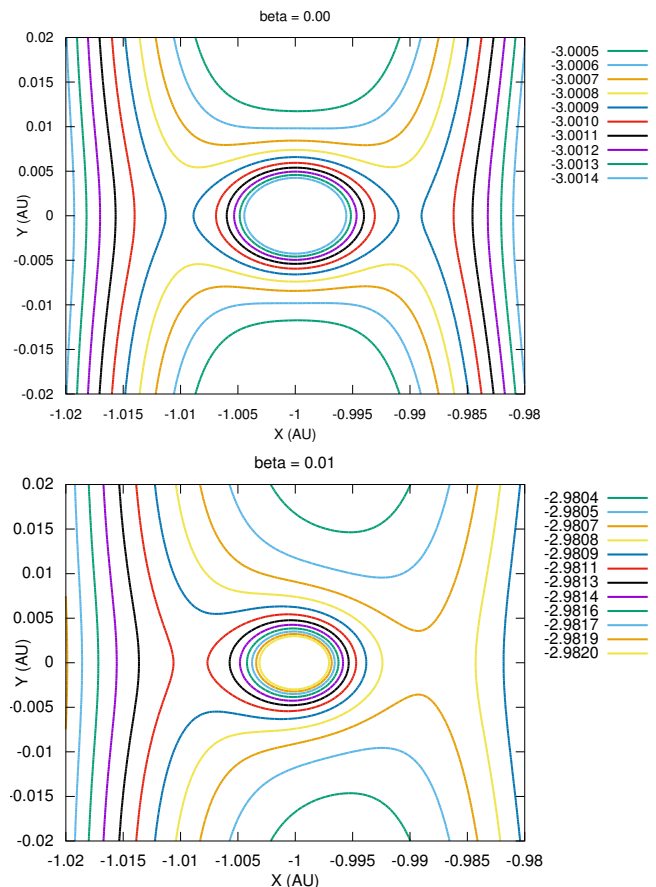


Fig. 1: Projection of the zero velocity curves in the x, y plane, $\mathcal{ZV}(J_c) = \{(x, y, 0) \in \mathbb{R}^3 \mid J_c + 2\tilde{\Omega}(x, y, 0) = 0\}$ for $\beta = 0.00$ (top) and $\beta = 0.01$ (bottom).

V. FAMILY OF EQUILIBRIUM POINT

It is well known¹⁴ that when the SRP is discarded ($\beta = 0$) the Earth-Sun RTBP has five equilibrium points: three of them

$(L_{1,2,3})$ are on the line joining the two primaries and are linearly unstable (saddle \times centre \times centre), while the other two ($L_{4,5}$) are on the ecliptic plane forming an equilateral triangle with the two primaries and are linearly stable (centre \times centre \times centre).

When the sail is perpendicular to the Sun-sail line ($\alpha, \delta = 0$) we have a similar portrait as for $\beta = 0$ we have five equilibrium points $SL_{1,\dots,5}$ slightly displaced towards the Sun w.r.t the classical Lagrangian points $L_{1,\dots,5}$. Three of them in the Earth-Sun line ($SL_{1,2,3}$) and unstable, and two forming a triangle with the two primaries ($SL_{4,5}$) and stable.¹⁰ Note that in this case we are essentially changing the magnitude of the Sun's attracting force.

When we change the sail orientation ($\alpha \neq 0$ or/and $\delta \neq 0$) we can artificially displace the equilibrium point. Variations in α will displace the points to one side or the other from the Sun-sail line, while variations in δ will displace the equilibrium points above or below the ecliptic plane.^{4,6,12}

In Fig. 2 we can see the family of equilibria on the xy -plane (i.e. for $\alpha \in [-\pi/2 : \pi/2]$ and $\delta = -\pi/2$) and $\beta = 0.01, 0.02, 0.03, 0.04$ and 0.05 , and in Fig. 3 we have a zoom of these families close to the Lagrangian points $L_{1,\dots,5}$. All these points have been computed using a continuation method w.r.t. one of the angles defining the sail orientation.

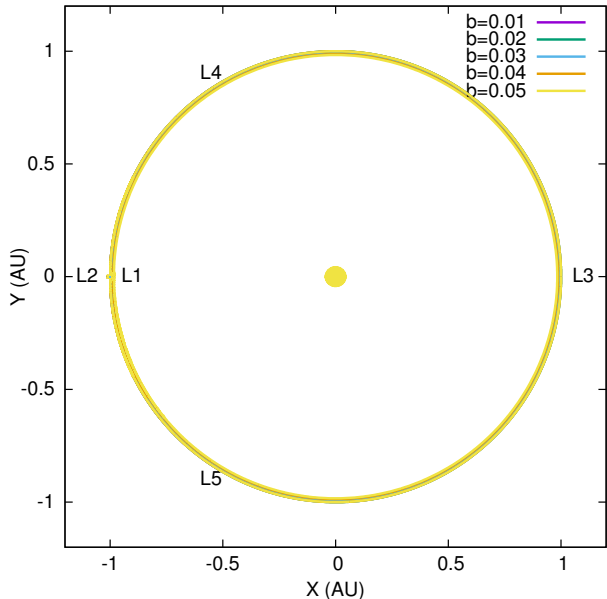


Fig. 2: Family of equilibrium points on the xy -plane ($z = 0$ and $\delta = -\pi/2$) for $\beta = 0.01, 0.02, 0.03, 0.04$ and 0.05 .

For small β ($\ll 10^{-5}$) we have five disconnected families of equilibrium points, each family parametrised by the two angles defining the sail orientation. As β grows ($\approx 10^{-5}$) the equilibria surfaces related to L_3, L_4 and L_5 merge into each other, having three disconnected families of equilibria (this is the case of $\beta = 0.01, 0.02$ in Figs. 2 and 3). Between $\beta = 0.02$ and 0.03 the surface related to L_1 merges with the large surface containing $L_{3,4,5}$, having only two disconnected surfaces of equilibria (as can be seen in Figs. 2 and 3 for $\beta = 0.03, 0.04$ and 0.05). The two remaining surfaces will never merge into each other as

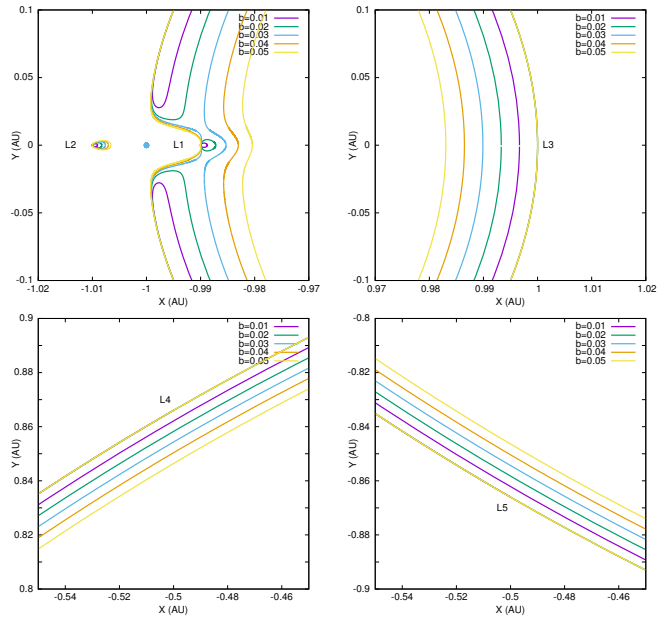


Fig. 3: Zoom around $L_{1,2}$ (top-left), L_3 (top-right), L_4 (bottom-left) and L_5 (bottom-right) for the family of equilibrium points on the xy -plane ($z = 0$ and $\delta = -\pi/2$) for $\beta = 0.01, 0.02, 0.03, 0.04$ and 0.05 .

there are some frontiers for the possible equilibria, given the sail orientation restrictions $\langle \mathbf{n}, \mathbf{r}_s \rangle > 0$, that separates them.^{10,11}

We can classify the equilibrium points according to their stability, which is given by the eigenvalues of the linearised flow around the equilibrium point. As the system is only Hamiltonian for a small set of sail parameters, there is no a priori bound between the pair of eigenvalues. We can distinguish three class of equilibrium points, \mathcal{T}_1 which are unstable and have as eigenvalues $\lambda_1 > 0, \lambda_2 < 0, \nu_1 \pm i\omega_1$ and $\nu_2 \pm i\omega_2$. Where $|\nu_{1,2}| \ll |\lambda_{1,2}|$ hence the main instability is given by the saddle. The class \mathcal{T}_2 are equilibria that have all their eigenvalues complex $\nu_{1,2,3} \pm i\omega_{1,2,3}$, and at least one of the real parts $|\nu_i| > 0.001$. This means that they present some instability given by a complex saddle. Finally the third class of equilibrium points \mathcal{T}_3 are almost stable, as all the eigenvalues are complex $\nu_{1,2,3} \pm i\omega_{1,2,3}$ and all the real parts $|\nu_{1,2,3}| < 0.001$. We call them almost stable as the required time to leave the vicinity of the equilibrium point is large. In Fig. 4 we show the relation between the position of the equilibrium point and the class where they belong. As we can see the equilibria close to L_1 and L_2 are unstable, as well as those close to L_3 .

We can also classify the equilibrium points by the required angle with respect to the Sun-sail direction to have equilibria. Although the angle between the sail normal vector and the Sun-sail line can vary between $[-\pi/2 : \pi/2]$, it is not feasible to consider $|\alpha| > \pi/4$ due to technical limitations. In Fig. 5 we plot the relation between the equilibrium position and the angle α , in green we have the points with $|\alpha| \leq \pi/4$ and purple those with $|\alpha| \geq \pi/4$. This gives us an idea of the points we can actually consider for mission applications. As we can see the points close to the classical Lagrange points $L_{1,\dots,5}$ are not useful as they re-

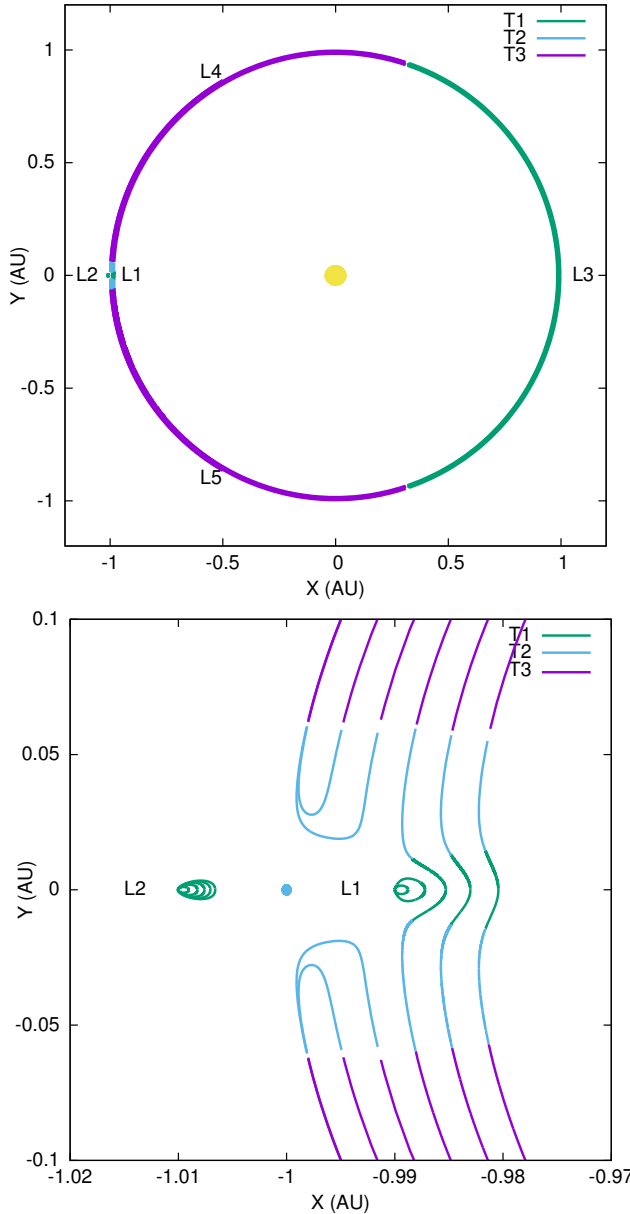


Fig. 4: Stability indicator for the family of equilibrium points on the xy -plane ($z = 0$ and $\delta = -\pi/2$) for $\beta = 0.01, 0.02, 0.03, 0.04$ and 0.05 . The class $\mathcal{T}_1, \mathcal{T}_2, \mathcal{T}_3$ are represented in colour green, blue and purple respectively.

quire $|\alpha| \approx \pi/2$, while their displaced ‘brothers’ $SL_{1,\dots,5}$ and the equilibria close to them can be useful.

These equilibrium points have been proposed as target positions for several mission applications,¹² the most relevant one is the Sunjammer mission. The missions proposed usually require to remain close to an equilibrium point, in this paper we want to see if the invariant manifolds associated to the unstable equilibrium points (class \mathcal{T}_1) can help us to drift along the family of equilibria in a controlled way or even provide natural transfer trajectories to go from one region to another.

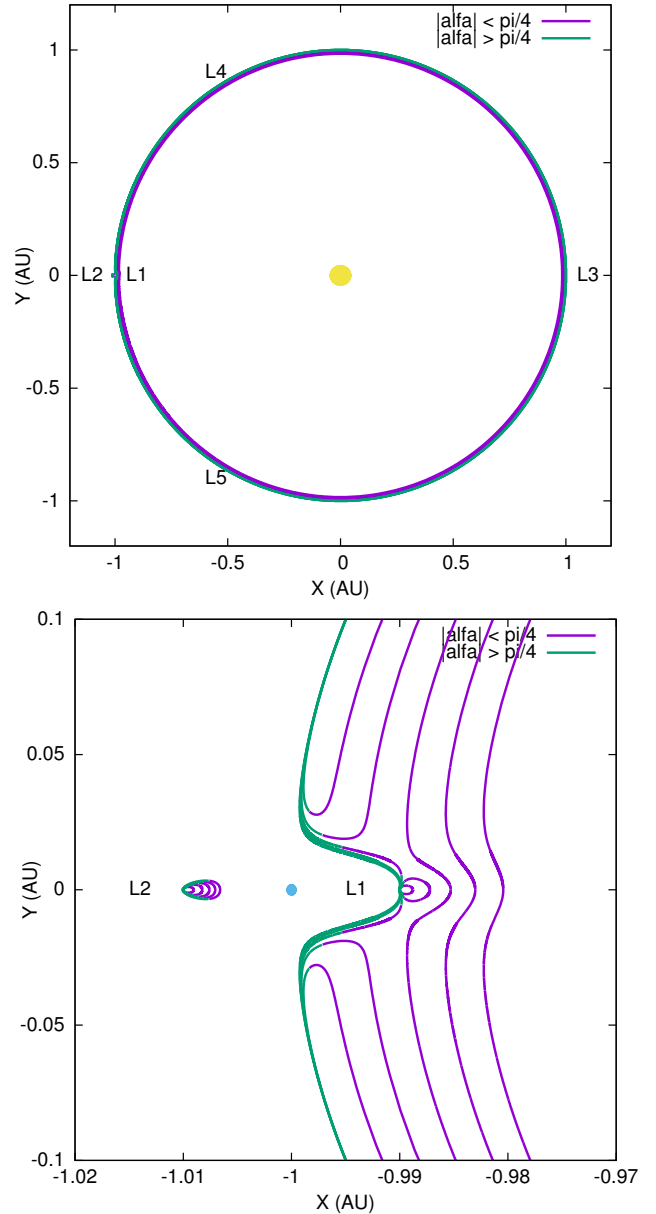


Fig. 5: Sail orientation relation between the family of equilibrium points on the xy -plane ($z = 0$ and $\delta = -\pi/2$) for $\beta = 0.01, 0.02, 0.03, 0.04$ and 0.05 . Green points present $|\alpha| \leq \pi/4$ and Purple points $|\alpha| \geq \pi/4$.

VI. SURFING WITH INVARIANT MANIFOLDS

The stable and unstable manifolds associated to family of periodic and quasi-periodic orbits have already been used to provide cheap transfer trajectories in the RTBP.⁹ When we consider the RTBPS we have a family of equilibrium points and their associated stable and unstable manifolds can also be used to have natural transfer trajectories.

We have focused on the equilibrium points of class \mathcal{T}_1 described in the previous section. As already mentioned, these points are unstable and have a saddle associated to them. We have computed for different equilibrium points (i.e. different sail orienta-

tion) their stable and unstable invariant manifolds and tried to see in a graphical way if there are connections between them. This will allow us to find transfer trajectories from one equilibrium point to the other.

In this section we will describe three mission options that the invariant manifolds structure provides us. The first mission focuses on performing small changes on the sail orientation moving along the stable and unstable manifolds of different equilibrium points drifting in a controlled way along the family of equilibria. The second mission is to find transfer trajectories from the vicinity of L_1 to the vicinity of L_2 . The third mission is to find transfer trajectories connection L_1 or L_2 with the stable Lagrangian points $L_{4,5}$.

VII.I Drift along the Family of Equilibria

Here we want to address the problem of finding a transfer strategy that allows us to go from the vicinity of one equilibrium point to another. For this purpose we will not use control theory algorithms but rather the information on the natural dynamics of the system. We will consider the two target equilibrium points to belong to the same connected component of the surface of equilibria and of class \mathcal{T}_1 . And derive a sequence of changes in the sail orientation that take the sail from one point (p_0) to the other (p_1).

As we know all the equilibrium points of class \mathcal{T}_1 are unstable and their linear dynamics can be well approximated by a saddle \times centre \times centre.^{5,7} Hence, a sail close to the equilibrium point will escape along the unstable direction, if we change the sail orientation the trajectory will escape along the new unstable direction. The main idea behind these strategies relies on understanding the position of the saddle on the phase space, and how this one varies when we vary the sail orientation. With this information we can be able to derive a sequence of changes on the sail orientation that will drive the satellite along the different saddles.

One can check that for the values of β that we have considered in this paper ($\beta = 0.01, \dots, 0.05$), and the equilibrium points that lie in the orbital plane ($z = 0$), the saddle projections does not vary much and the family of equilibrium points moves in between the stable and unstable directions. In Fig. 6 we can appreciate this phenomena for $\beta = 0.03$. There we have plotted the family of equilibrium points and the projection of the stable and unstable directions in the xy -plane.

Now that we know how the stable and unstable directions vary along the family we can use this to derive a ‘surfing strategy’. First we need to track the trajectory of the sail in the saddle plane, and when we are far from the equilibrium point, change the sail orientation so that the trajectory of the sail will move along the stable manifold of the new fixed point and then escape along its unstable manifold. We will repeat this process until we reach a vicinity of the final target point. During all these process we must also take into account the projection of the trajectory in the other centre directions. There we will have a sequence of rotations along different equilibrium points and this might result

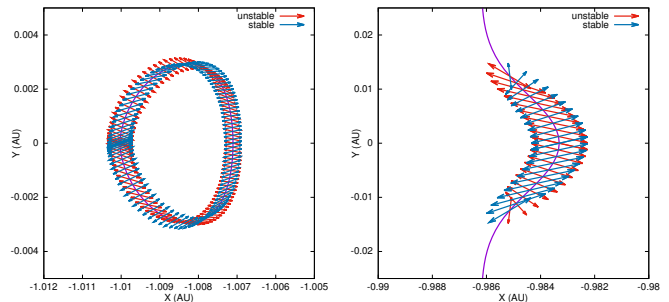


Fig. 6: xy -projection of the family of equilibrium points for $\beta = 0.03$ and the stable and unstable vectors for the equilibrium points in the SL_1 family (right) and the SL_2 family (left).

unbounded. In Fig. 7 we have a schematic representation of the strategy that we have just explained.

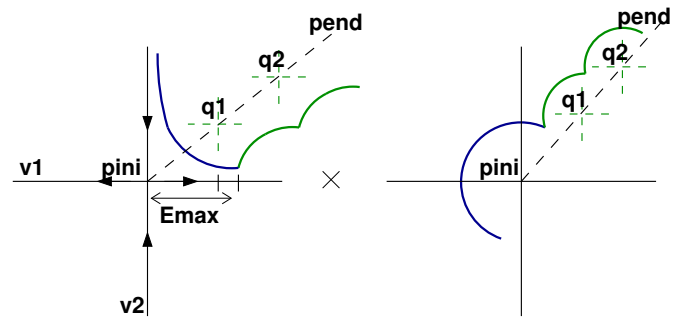


Fig. 7: Schematic representation of the surfing strategy.

In previous works^{5,7} we have tested these strategies for different missions scenarios, being able to move along the family of equilibria in a controlled way. There you can also find more details and information on the practical implementation of the strategies. We must mention that the trajectories that we find using these ideas might not be optimal in terms of transfer time, but they will tell us if a transfer between two points is possible and can also be used as initial guesses for an optical control scheme.

As an example mission we have selected two equilibrium points in the ecliptic plane slightly displaced from the Earth-Sun line: $p_0 = (-9.8558558e-01, -3.2243367e-03, 0.000000e-00)$ for $\alpha_0 = 9.9947e-02\text{rad} \approx 5.73^\circ$ and $\delta = -\pi/2$, and $p_1 = (-9.8558558e-01, 3.2243367e-03, 0.000000e-00)$ for $\alpha = -9.9947e-02\text{rad} \approx 5.73^\circ$ and $\delta = -\pi/2$. We have used surfing scheme discussed above to find a sequence of changes on the sail orientation that lead the trajectory of the sail from p_0 to p_1 .

In Fig. 8 we can see the projection in the xy -plane of this trajectory that the sail follows to go from p_0 to p_1 . As we can see the trajectory remains close to the family of equilibrium points.

In Fig 9 we can see a part of the trajectory that the sail follows projected in the saddle and centre planes of p_0 . Looking at the saddle projection (left) we can clearly see how the trajectory moves along the different saddles that appear each time we change the sail orientation. The trajectory on the centre projections (right) rotates around the different equilibrium points.

Finally in Fig. 10 we can see the variation of the sail orientation α over time. Where we can clearly see how the sail orientation varies in a discrete way, and goes from 5.73° to -5.73° , the sail orientation corresponding to the equilibrium points. As the two points p_0 and p_1 the trajectory will always lie in the plane, $z = 0$, and $\delta \approx -\pi/2$ throughout the entire transfer trajectory.

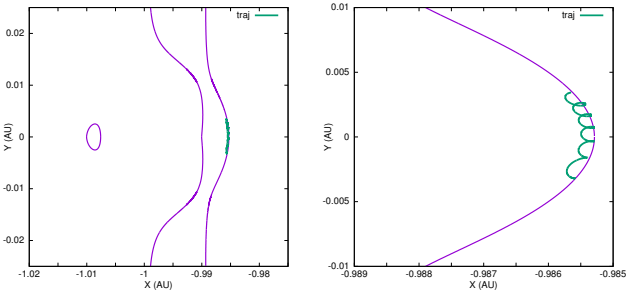


Fig. 8: xy projection of the solar sail trajectory during the surfing strategy.

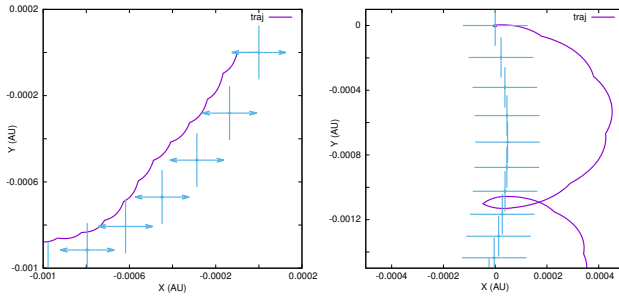


Fig. 9: Saddle and Centre projections of the solar sail trajectory during the surfing strategy.

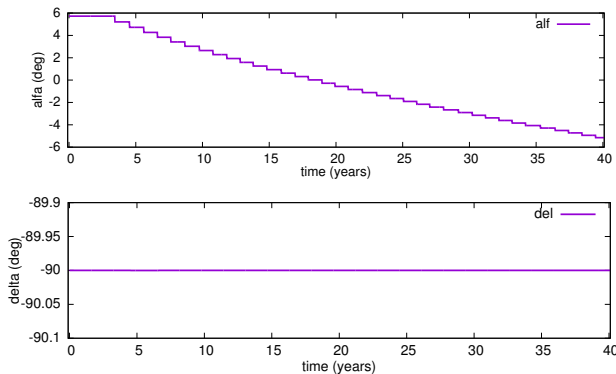


Fig. 10: Variation of the angles defining the sail orientation through time during the surfing strategy, α (top) δ (bottom)

VI.II Surfing from SL_1 to SL_2

The transfer strategies that we have described in the previous section use the information on the local dynamics of an equilibrium point, and allow us only to move inside one of the connected components of the surfaces of equilibria. For instance,

if we want to move from a vicinity of SL_1 to a vicinity of SL_2 we need to compute the whole stable and unstable manifolds and see if they can lead us there.

We have considered $\beta = 0.01$ and $\beta = 0.03$, two values of β where the structure of the family of equilibrium points close to SL_1 and SL_2 are different (see section V.). For each β we have taken a set of 100 points in the family and for each point and its corresponding sail orientation (α, δ fixed) we have computed their stable and unstable invariant manifolds. We have integrated each of them up to 20UT≈ 3.2 years.

In Fig. 11 we show the projection in positions of the stable and unstable manifolds related to SL_1 and SL_2 (the displaced Lagrangian points for $\alpha = 0$) for $\beta = 0.01$ (top) and $\beta = 0.03$ (bottom). In the first case ($\beta = 0.01$) we see that we can find intersections between the stable and unstable manifolds of SL_1 and SL_2 , while this is not true for $\beta = 0.03$. Nevertheless, we need to be careful to avoid the a possible collision with the Earth.

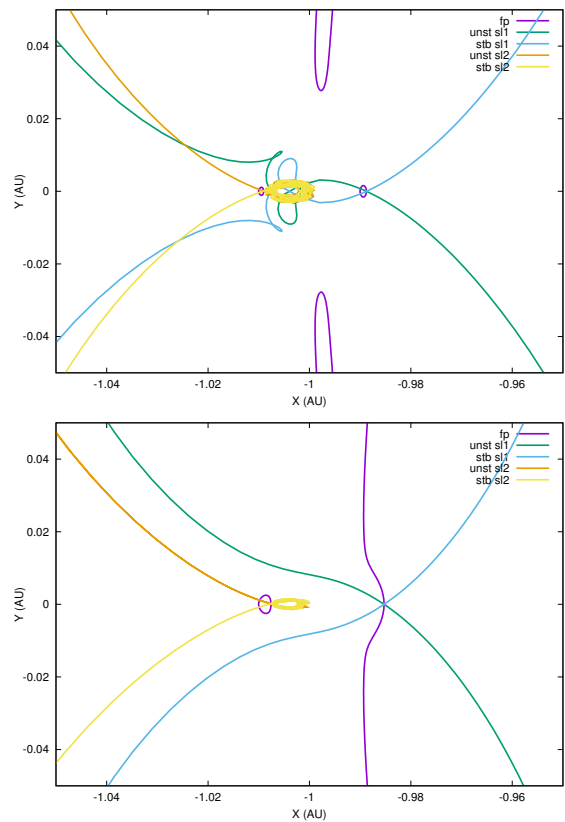


Fig. 11: xy -projection of the stable and unstable manifolds from SL_1 and SL_2 for $\beta = 0.01$ (top) and $\beta = 0.03$ (bottom).

Moreover, if we want to find a transfer trajectory between the two points, we need that the stable and unstable manifolds match not only in positions, but also in energy level (or the \tilde{J}_c value). As we discussed in section IV. for $\alpha = 0$ or α small \tilde{J}_c varies very little and defines the frontiers of possible motion. We need the intersections to happen also at the same J_c value to be sure that the trajectory will follow the new stable manifold.

In Fig. 12 we plot for $\beta = 0.01$ the trajectories of the stable and

unstable manifolds. Here the $x - y$ coordinates correspond to the position and the z coordinate to the energy value of each point (Eq. 5). We can see that for $\alpha = 0$ the trajectories from SL_1 to SL_2 do not match in energy (top). But if we move along the family of equilibria in the SL_1 family (by varying the sail orientation) we can lower the energy and find different intersections. In Fig. 13 we show a similar structure but for $\beta = 0.03$, although in this case it is harder to find intersections in positions.

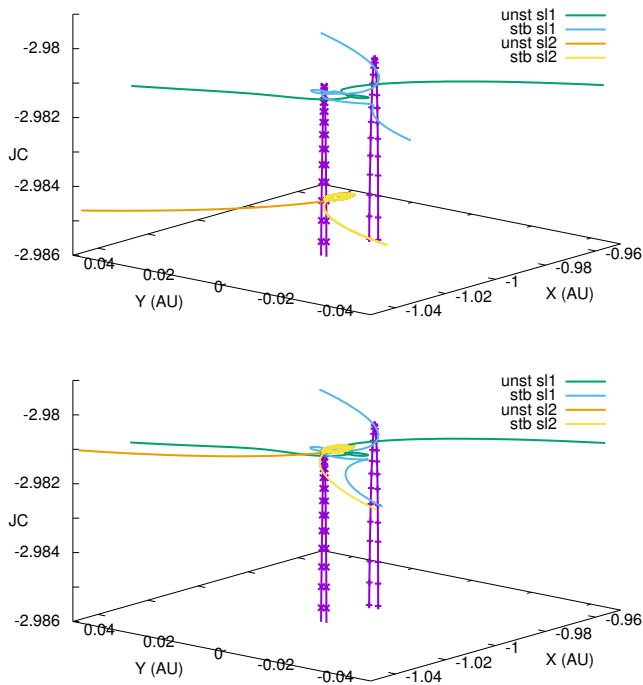


Fig. 12: Projection in the x, y, J_c space of the stable and unstable manifolds from the equilibrium points in the L_1 and L_2 family for $\beta = 0.01$. Top: case where there is no intersection in energy (J_c), Bottom: case where we have an intersection in energy.

A more extensive exploration should be done to find all possible intersections between the different families for different realistic sail configurations. But these results show that a transfer between SL_1 and SL_2 is possible and that it is more feasible for low performance solar sails. We also need to study in more detail how to perform the transfer strategy in order to, with the solar sail, transfer from one manifold to the other. This last part is work in progress.

VI.III Surfing from SL_1/SL_2 to $SL_{4,5}$

It is well known that the equilateral Lagrangian points $L_{4,5}$ are linearly stable and have around them a large stability region, where a spacecraft placed in this region will remain there, without the need of control, for more than 1000 years. Their positions are also very interesting as we could monitor the Sun's activity free of interference. If we could have three probes, one at L_1 and the other two at L_4 and L_5 respectively we can have a 3D monitoring of the Sun. Accessing to this regions with a regular spacecraft is

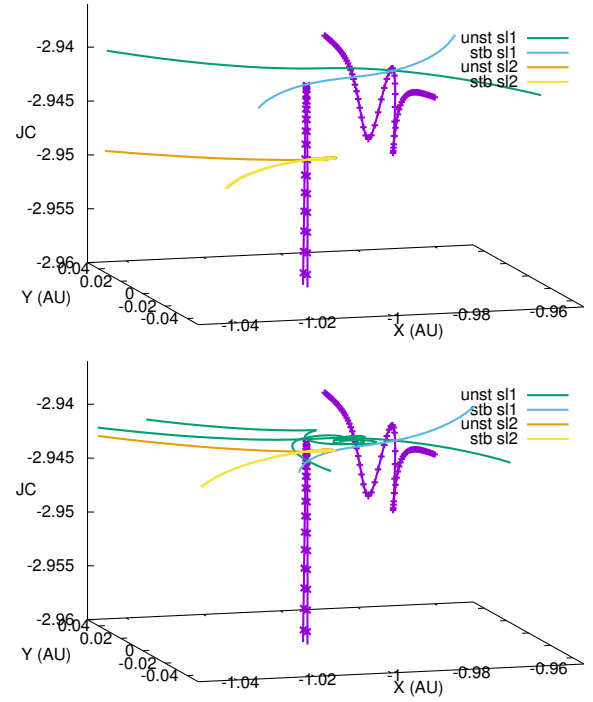


Fig. 13: Projection in the x, y, J_c space of the stable and unstable manifolds from the equilibrium points in the L_1 and L_2 family for $\beta = 0.03$. Top: case where there is no intersection in energy (J_c), Bottom: case where we have an intersection in energy.

very expensive as they require a large Δv . Here we want to see if by moving the sail orientation we are able to gain energy in a continuous way to reach the region of L_4 or SL_4 in a reasonable time.

As before we have taken a set of 100 equilibrium points close to SL_1 and SL_2 of class T_1 for $\beta = 0.01$ and 0.03. For each point and its associated sail orientation we have computed their stable and unstable manifolds up to 20UT ≈ 3.2 years. Then we look if there are intersections in position and J_c with the $SL_{4,5}$ vicinity.

In Fig. 14 we show the projection on the xy -plane of the invariant manifolds associated to SL_1 and SL_2 for $\beta = 0.01$ (top) and $\beta = 0.03$ (bottom). As we can see in both cases these trajectories come close to L_4 . The main difference between them is the time required to reach the vicinity of L_4 . For $\beta = 0.01$ the time of flight between SL_1 and SL_2 is quite similar, while for $\beta = 0.03$ departing from SL_2 is faster. This is mainly because as β increases SL_2 becomes more unstable while SL_1 loses instability, in other words the real eigenvalue related to SL_2 grows with β while the real eigenvalue related to SL_1 decreases.

On the other hand, as we have already mentioned, we must have a match in energy (J_c) in order to have feasible transfers trajectories to the L_4 vicinity and remain there. If we use the invariant manifolds associated to SL_1 and SL_2 (equilibrium points for $\alpha = 0$), we have no energy drift, as the system is Hamiltonian. We can see this in Fig. 15 for the transfers from SL_1 and Fig. 16 for the transfers from SL_2 . In both plots $\beta = 0.01$ (top) and $\beta = 0.03$ (bottom).

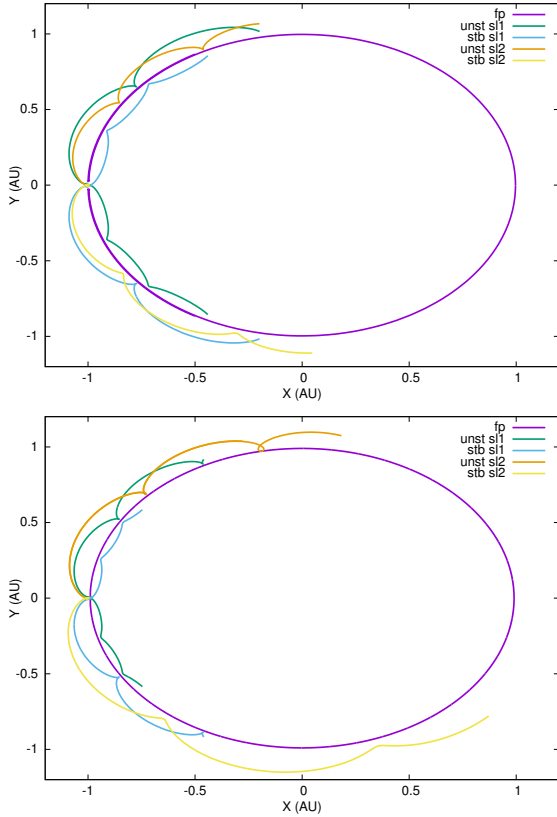


Fig. 14: xy -projection of the stable and unstable manifolds from SL_1 and SL_2 for $\beta = 0.01$ (top) and $\beta = 0.03$ (bottom)

If we consider a sail orientation, $\alpha \neq 0$ we will have an energy drift as discussed in section IV.. We can find stable and unstable manifolds, given by certain sail orientations, where J_c increases until it reaches $J_c(L_4)$. But we need to be careful in selecting the angles as in some cases the stable and unstable manifolds get trapped in the vicinity of other equilibria far from L_4 .

In Fig. 17 we show the 3D projections of the invariant manifolds (x, y, J_c) for $\beta = 0.01$ associated equilibrium points in the SL_1 family (top) and the SL_2 family (bottom) that reach the energy of SL_4 . In Fig. 18 we have selected equilibrium points related to both families where the trajectories get trapped close to another equilibrium point and do not reach the vicinity of L_4 .

Here we have studied the possibility of finding transfer trajectories that reach the region close to L_4/L_5 with the desired energy level, having a constant drift due to the sail. We have found trajectories that reach there, showing that a transfer is possible. We still need to do a more detailed study on the range of sail orientations that take us there, and how to get captured in the L_4/L_5 region once we get there.

VII. CONCLUSIONS

In this paper we have done a preliminary study on the possibilities that the stable and unstable manifolds associated to the artificially equilibria have to derive transfer orbits between regions

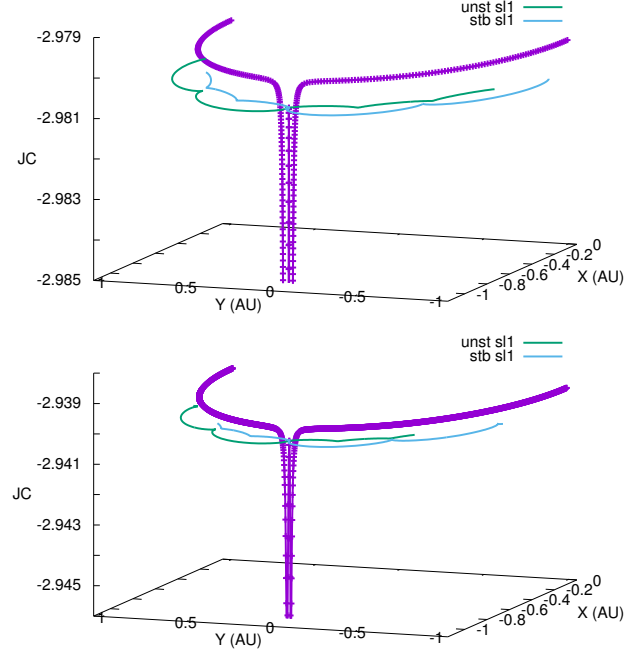


Fig. 15: Projection in the x, y, J_c space of the stable and unstable manifolds from the equilibrium points in the SL_1 for $\beta = 0.01$ (top) and $\beta = 0.03$ (bottom). The points correspond to the family of equilibrium point and their associated energy. In both cases there is no intersection in energy (J_c) with the L_4 region.

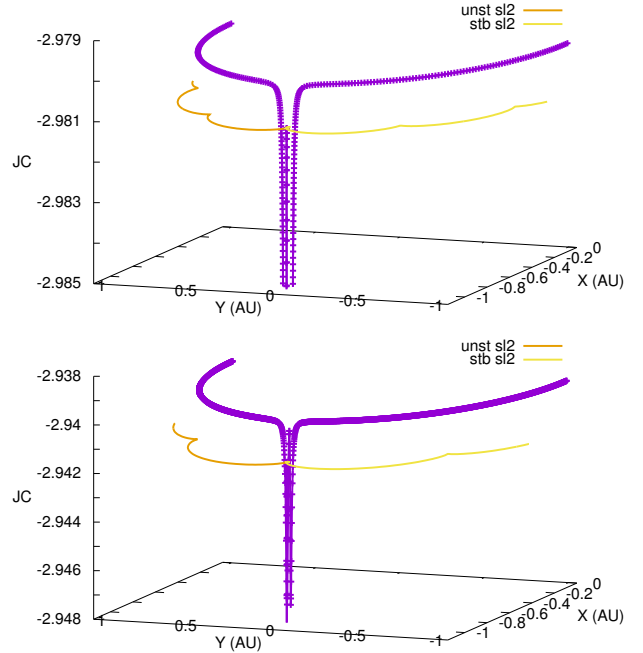


Fig. 16: Projection in the x, y, J_c space of the stable and unstable manifolds from the equilibrium points in the SL_2 for $\beta = 0.01$ (top) and $\beta = 0.03$ (bottom). The points correspond to the family of equilibrium point and their associated energy. In both cases there is no intersection in energy (J_c) with the L_4 region.

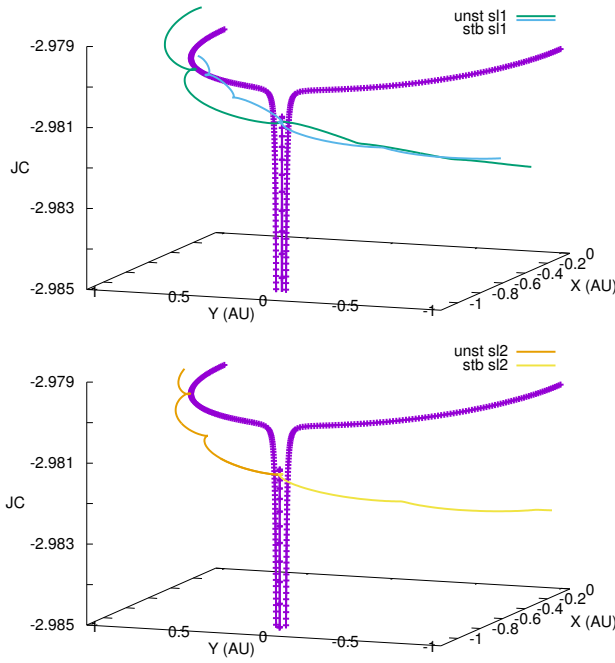


Fig. 17: Projection in the x, y, J_c space of the stable and unstable manifolds from the equilibrium points in the SL_1 (top) and L_2 (bottom) for $\beta = 0.01$. The points correspond to the family of equilibrium point and their associated energy. In both cases we see that there is an intersection with the energy (J_c) of the L_4 region.

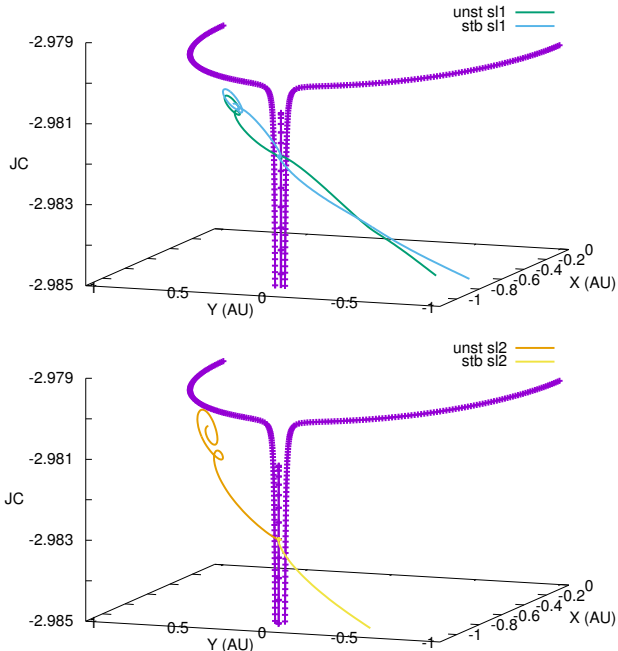


Fig. 18: Projection in the x, y, J_c space of the stable and unstable manifolds from the equilibrium points in the SL_1 (top) and L_2 (bottom) for $\beta = 0.01$. The points correspond to the family of equilibrium point and their associated energy. In both cases we see how the unstable invariant manifold gets trapped before reaching the L_4 region.

in the phase space.

First of all in section V. we have reviewed the family of artificial equilibria that appear in the RTBP for different sail orientations and performances $\beta = 0.01, 0.02, 0.03, 0.04$ and 0.05 . We have discussed their position in the phase space as well as some of their characteristics.

In section VI.I we have studied the possibilities that the linear dynamics of the unstable equilibrium points give us to derive strategies to drift along the family of equilibria.

In sections VI.II and VI.III we have selected different equilibrium points and for each of them we have computed their stable and unstable manifolds and see if we can find connections between the SL_1 , SL_2 and SL_4 regions. We have seen that there exist connections between SL_1 to SL_2 for low performance solar sails ($\beta = 0.01, 0.02$). For any value of β we have connections between $SL_{1,2}$ and $SL_{4,5}$, although here the larger the solar sail is the faster we will arrive there.

We must mention that this is a preliminary study but shows promising results. Further explorations should be made to measure for each β the range of sail orientations that allow us to perform the different transfers, as well as the manoeuvres required to change from one invariant manifold to the other.

Acknowledgement

This work has been supported by the MEC grant MTM2012-32541, the AGAUR grant 2014 SGR 1145 and the AGAUR postdoctoral fellowship Beatriu de Pinós (BP-B 00142-2011).

References

- [1] M. Ceriotti and C. McInnes. Natural and sail-displaced doubly-symmetric lagrange point orbits for polar coverage. *Celestial Mechanics and Dynamical Astronomy*, 114(1-2):151–180, 2012.
- [2] B. Dachwald, H. Boehnhardt, U. Broj, U.R.M.E. Geppert, J-T Grundmann, W. Seboldt, P. Seefeldt, P. Spiegel, L. Johnson, E. Kührt, S. Mottola, M. Macdonald, C. McInnes, M. Vasile, and R. Reinhard. Gossamer roadmap technology reference study for a multiple neo rendezvous mission. In Malcolm Macdonald, editor, *Advances in Solar Sailing*, Springer Praxis Books, pages 211–226. Springer Berlin Heidelberg, 2014.
- [3] B. Dachwald, W. Seboldt, M. Macdonald, G. Mengali, A.A. Quarta, C.R. McInnes, L. Rios-Reyes, D.J. Scheeres, B. Wie, M. Görlich, et al. Potential Solar Sail Degradation Effects on Trajectory and Attitude Control. In *AIAA Guidance, Navigation, and Control Conference and Exhibit*, volume 6172, 2005.
- [4] A. Farrés. *Contribution to the Dynamics of a Solar Sail in the Earth-Sun System*. PhD thesis, Universitat de Barcelona, 2009.

- [5] A. Farrés and À. Jorba. Solar sail surfing along families of equilibrium points. *Acta Astronautica*, 63:249–257, July–August 2008.
- [6] A. Farrés and À. Jorba. Periodic and quasi-periodic motions of a solar sail around the family SL_1 on the Sun-Earth system. *Celestial Mechanics and Dynamical Astronomy*, 107:233–253, 2010.
- [7] A. Farrés and À. Jorba. Dynamical system tools to navigate in the earth-sun system. In *Proceedings of the XXIV congress on differential equations and applications*, Cadiz, Spain, June 2015.
- [8] J. Heiligers, B. Diedrich, B. Derbes, and C. McInnes. Sunjammer : Preliminary end-to-end mission design. In *Proceedings of the AIAA/AAS Astrodynamics Specialist Conference 2014*, 2008.
- [9] W.S. Koon, M.W. Lo, J.E. Marsden, and S.D. Ross. *Dynamical Systems, the Three-Body Problem and Space Mission Design*. Interdisciplinary Applied Mathematics. Springer New York, 2011.
- [10] A. McInnes. Strategies for solar sail mission design in the circular restricted three-body problem. Master's thesis, Purdue University, August 2000.
- [11] C.R. McInnes. *Solar Sailing: Technology, Dynamics and Mission Applications*. Springer-Praxis, 1999.
- [12] C.R. McInnes, A.J.C. McDonald, J.F.L. Simmons, and E.W. MacDonald. Solar sail parking in restricted three-body system. *Journal of Guidance, Control and Dynamics*, 17(2):399–406, 1994.
- [13] S. Soldini, C. Colombo, and S. Walker. The end-of-life disposal of satellites in libration-point orbits using solar radiation pressure. *Advances in Space Research*, pages –, 2015.
- [14] V. Szebehely. *Theory of orbits. The restricted problem of three bodies*. Academic Press, 1967.
- [15] L. Visagie, V. Lappas, and S. Erb. Drag sails for space debris mitigation. *Acta Astronautica*, 109:65 – 75, 2015.